DOI: 10.1002/ejic.201100091

Syntheses, Crystal Structures, and Optical Properties of Indium Arsenic(III) Oxide Halides: $In_2(As_2O_5)Cl_2$ and $In_4(As_2O_5)(As_3O_7)Br_3$

Xiao-Ming Jiang,[a,b] Zhong-Ning Xu,[a] Zhong-Yan Zhao,[a] Sheng-Ping Guo,[a] Guo-Cong Guo,*[a] and Jin-Shun Huang[a]

Dedicated to Professor John D. Corbett on the occasion of his 85th birthday

Keywords: Layered compounds / Indium / Arsenic / Halides / Optical properties

Two new indium arsenic(III) oxide halides, $In_2(As_2O_5)Cl_2$ (**1**) and $In_4(As_2O_5)(As_3O_7)Br_3$ (**2**), have been prepared by solid-state reaction. Both of the compounds feature layered structures, in which indium–oxide halide octahedral rings or indium–oxo chains are bridged by indium–oxide halide octahedral dimers or indium–oxo unicapped trigonal prisms, and the interlinkage between the rings or chains is also consolidated by $(As_2O_5)^{4-}$ anions for **1**, or $(As_2O_5)^{4-}$ and $(As_3O_7)^{5-}$ anions for **2**. Compound **2** is the first compound in which three different indium-ion coordination geometries coexist with the In^{3+} cations coordinated by O^{2-} and Br^- to form $[InO_6]$, $[InO_7]$, and $[InOBr_3]$ units. The diffuse reflectance spectra and band-structure calculations show that they are wide-band-gap semiconductors.

Introduction

Metal oxide halide compounds that contain so-called lone-pair cations with stereochemically active electron pairs such as Te^{4+}, Se^{4+}, Sb^{3+}, and As^{3+} have been shown to form a group of compounds with a high probability for novel materials with low-dimensional crystal structures and excellent chemical and physical properties, such as second-order nonlinear optical (NLO), magnetic, and luminescent properties, and so on.[1–7] The active electron pairs in lone-pair cations always "push" the oxide ligands toward one side of the cation, thus leading to a highly asymmetric coordination geometry, which is essential to the discovery of new NLO materials.[2] Crystal structures are often opened up by terminal halogen atoms as well as lone-pair cations, which are likely to form bonds only with O in oxide halogenides to make the metal cations take low-dimensional arrangements.[3] The low-dimensional crystal structure may be very important for some special magnetic materials, such as unconventional magnetic instability, ground-state order, spin-lattice coupling, halogen-mediated exchange, incommensurate magnetic ordering, and so on, in a metal oxide halogenide system.[4,5] Metal cations contribute to the good performances of materials, whereas lone-pair cations and halogens are in favor of forming "nice" structures, though the relationship between structure and performance is always complicated. Transition- and rare-earth-metal ions, which are magnetically susceptible, can form some novel low-dimensional quantum-spin systems like $M_aL_bX_c$ (M = Fe, Co, Ni, Cu; L = SeO_3, TeO_3, TeO_5; X = Cl, Br; a = 2, 5; b = 1, 4; c = 1, 2).[5] Alkali (or alkaline earth) metal ions of high polarization and d^0 transition ions can form good NLO materials with large second-harmonic generation (SHG) efficiencies; these include $Na_2Mo_3Te_3O_{16}$, $Na_2W_2TeO_9$, $BaMo_2TeO_9$, and $M_2W_3TeO_{12}$ (M = Rb, Cs).[6] Rare-earth-metal ions, which have several different energy levels, can also form luminescent materials like $Ln_5MTe_7O_{23}Cl_3$ (Ln = Pr, Nd; M = Mo, W).[7] To the best of our knowledge, although many oxide halogenide compounds that contain lone-pair cations have been prepared (those containing Se^{4+} and Te^{4+} in particular have received a great deal of attention[3,8]), and most metal ions in such types of compounds are transition- and rare-earth-metal ions, relatively few of them are found to contain group-15 elements. In particular, the only known oxide halogenide compounds that contain As^{3+} are oxoarsenate(III) chloride compounds[9] of lead and neodymium like $Pb_6Cu(AsO_3)_2Cl_7$[9e] and $Nd_5(AsO_3)_4Cl_3$,[9f] and oxoarsenate(III) oxide chloride compounds[10] of lead and some rare-earth elements like $Ln_3(AsO_3)_2OCl$ (Ln = La, Sm, Gd)[10a] and $Pb_8Cu(AsO_3)_2O_3Cl_5$.[10f] Herein we report two indium oxide halogenide compounds that contain lone-pair As^{3+}, $In_2(As_2O_5)Cl_2$ (**1**) and $In_4(As_2O_5)$-

[a] State Key Laboratory of Structural Chemistry, Fujian Institute of Research on the Structure of Matter, Chinese Academy of Sciences,
Fuzhou 350002, P. R. China
Fax: +86-591-8371-4946
E-mail: gcguo@fjirsm.ac.cn
[b] Graduate School of Chinese Academy of Sciences,
Beijing 100039, P. R. China

Supporting information for this article is available on the WWW under http://dx.doi.org/10.1002/ejic.201100091.

$(As_3O_7)Br_3$ (**2**). Indium ions in **2** adopt three different coordination geometries, and UV/Vis/NIR diffuse reflectance spectroscopy as well as band structure calculations show that they are wide-band-gap semiconductors.

Results and Discussion

Structure Description

Compounds **1** and **2** crystallize in the triclinic system with space group $P\bar{1}$. Experimental parameters, atomic coordinates, and selected interatomic distances are listed in Tables 1, 2, and 3, respectively. They both show layered structures but have totally different building blocks.

Table 1. Crystal data and structure refinement parameters.

	1	**2**
Chemical formula	$In_2(As_2O_5)Cl_2$	$In_4(As_2O_5)(As_3O_7)Br_3$
M_r	530.38	1265.61
Crystal size [mm]	$0.10\times0.05\times0.01$	$0.15\times0.10\times0.02$
Crystal system	triclinic	triclinic
Space group	$P\bar{1}$	$P\bar{1}$
a [Å]	6.6957(12)	7.998(6)
b [Å]	7.4580(18)	10.523(6)
c [Å]	8.9568(19)	11.952(8)
α [°]	108.434(9)	70.92(2)
β [°]	104.983(2)	79.62(2)
γ [°]	102.045(4)	80.27(3)
V [Å^3]	388.77(14)	928.5(10)
Z	2	2
$D_{calcd.}$ [g cm^{-1}]	4.531	4.527
μ [mm^{-1}]	15.031	20.250
$F(000)$	476	1124
θ range [°]	2.56–25.00	2.06–25.50
Measd. reflections	2697	6256
Indep. reflections/R_{int}	1335/0.1125	3451/0.0572
Obsd. reflections	827	2628
R_1[a] [$I>2\sigma(I)$]	0.0630	0.0483
wR_2[b] (all data)	0.1773	0.1083
GOF on F^2	0.975	0.970
$\Delta\rho_{max}/\Delta\rho_{min}$ [e Å^{-3}]	2.495/–2.739	1.476/–1.829

[a] $R_1 = ||F_o| - |F_c||/|F_o|$. [b] $wR_2 = [w(F_o^2 - F_c^2)^2]/[w(F_o^2)^2]^{1/2}$.

Table 2. Atomic coordinates and equivalent isotropic displacement parameters [Å^2].

	x	y	z	U_{eq}[a]
1				
In1	0.59956(10)	0.30445(8)	0.47609(9)	0.0128(2)
In2	0.14796(10)	0.22570(9)	0.66220(9)	0.01236(19)
As1	0.10931(15)	0.15471(12)	0.24572(12)	0.0120(3)
As2	0.29837(15)	0.77117(12)	0.20106(12)	0.0121(3)
Cl1	0.7642(4)	0.3881(3)	0.2806(3)	0.0189(7)
Cl2	0.2485(4)	0.2895(3)	0.9576(3)	0.0255(8)
O1	0.1648(9)	0.7318(8)	0.3421(8)	0.0120(17)
O2	0.4638(9)	0.2121(8)	0.6506(7)	0.0129(19)
O3	0.3385(10)	0.0381(9)	0.2656(8)	0.0192(18)
O4	0.3145(10)	0.3794(9)	0.3850(8)	0.0177(19)
O5	0.0045(10)	0.0941(8)	0.3961(8)	0.0130(18)
2				
In1	0.0000	0.5000	0.0000	0.0118(3)
In2	0.0000	0.0000	0.0000	0.0119(3)
In3	0.25950(11)	0.21023(9)	0.01313(8)	0.0121(2)
In4	0.65161(11)	0.29032(9)	0.01227(8)	0.0124(2)
In5	0.15362(13)	0.19910(10)	0.52284(9)	0.0216(3)
As1	0.02775(16)	0.67955(13)	0.19629(11)	0.0119(3)
As2	0.25471(17)	0.37816(13)	0.22828(12)	0.0137(3)
As3	0.62440(16)	0.47832(13)	0.18240(11)	0.0127(3)
As4	0.92460(17)	0.08979(14)	0.25407(12)	0.0145(3)
As5	0.39772(17)	0.00754(13)	0.81718(12)	0.0131(3)
Br1	0.0988(2)	0.64462(18)	0.55427(16)	0.0403(4)
Br2	0.2646(2)	0.03008(18)	0.41125(15)	0.0383(4)
Br3	0.3889(2)	0.32329(19)	0.52747(18)	0.0464(5)
O1	0.1628(11)	0.3456(9)	0.1226(7)	0.0130(19)
O2	0.2411(10)	0.0815(8)	0.9111(7)	0.0118(19)
O3	0.7762(11)	0.4075(8)	0.0829(7)	0.0128(19)
O4	0.1355(11)	0.8051(8)	0.0814(7)	0.0130(19)
O5	0.4722(10)	0.3856(9)	0.1491(8)	0.0139(19)
O6	0.5620(11)	0.6384(8)	0.0847(8)	0.016(2)
O7	0.2162(11)	0.5606(9)	0.1736(8)	0.0152(19)
O8	0.0929(11)	0.3638(8)	0.8962(7)	0.0130(19)
O9	0.4986(11)	0.1218(9)	0.0708(8)	0.018(2)
O10	0.0668(11)	0.0873(8)	0.1214(7)	0.0135(19)
O11	0.0866(13)	0.0833(9)	0.6926(8)	0.022(2)
O12	0.7282(11)	0.1227(8)	0.1781(8)	0.0147(19)

[a] U_{eq} is defined as one-third of the trace of the orthogonalized U_{ij} tensor.

Compound **1** is the first oxoarsenate(III) chloride of indium, in which there are two crystallographically independent indium atoms, as shown in Figure S3a in the Supporting Information. The In1 atom is coordinated by five oxygen atoms with the bond lengths ranging from 2.084(7) to 2.244(5) Å and by one chlorine atom with the bond length of 2.464(3) Å, to form a distorted [$In1O_5Cl$] octahedron, two of which share edges with each other to form an In1 octahedral dimer. The In2 atom is also octahedrally coordinated by four oxygen atoms with bond lengths in the range 2.124(6)–2.219(6) Å and by two chlorine atoms with bond lengths of 2.666(2) and 2.414(3) Å, respectively, to form a distorted [$In2O_4Cl_2$] octahedron, two of which also share edges with each other to form an In2 octahedral dimer. Two In1 octahedral dimers are double-bridged by two In2 atoms to form a 12-membered ring; they share the In1 octahedral dimers with each other to form a ring chain along the a direction. The ring chains are interlinked through the In2 octahedral dimers along the b direction to form a 2D indium oxochloride layer (Figure 1). Meanwhile, atoms As1 and As2 are located between the ring chains and consolidate the interlinkage of chains through the formation of $(As_2O_5)^{4-}$ anions (Figure 2). The layers are stacked parallel along the c direction to yield the crystal structure of **1** (Figure 3).

There are five crystallographically different indium atoms in **2** (Figure S3b in the Supporting Information). Atoms In1, In2, and In3 are all octahedrally coordinated by six oxygen atoms to form distorted [InO_6] octahedra, which share edges with each other to form a 1D zigzag In octahedral chain that extends along the b direction (Figure 4). All the chains are edge- and corner-connected by distorted unicapped trigonal prism ($In4O_7$), in which the atom In4 is coordinated by seven oxygen atoms, to form a 2D indium oxide layer. The In–O bonds in [InO_6] and [InO_7] range from 2.110(8) to 2.341(8) Å, which lie in the normal range for In–O bond lengths in known indium oxides.[11] Meanwhile, atoms As1, As2, and As3 locate be-

Table 3. Select bond lengths [Å].[a]

1			
In1–O1#1	2.084(6)	As1–O5	1.804(8)
In1–O4	2.133(7)	As1–O3	1.912(7)
In1–O4#1	2.156(6)	As2–O2#1	1.742(6)
In1–O2	2.213(7)	As2–O1	1.786(7)
In1–O3	2.244(5)	As2–O3#5	1.827(6)
In1–Cl1	2.464(3)	O1–In2#3	2.175(6)
In2–O5	2.124(6)	O2–In2	2.166(7)
In2–O2	2.166(7)	O3–As2#4	1.827(6)
In2–O1#3	2.175(6)	O3–As1	1.912(7)
In2–O5#2	2.219(6)	O3–In1	2.244(5)
In2–Cl2	2.414(3)	O4–In1#1	2.156(6)
In2–Cl1#1	2.666(2)	O5–In2	2.124(6)
As1–O4	1.756(5)	O5–In2#2	2.219(6)
2			
In1–O3#6	2.110(8)	In5–Br1#7	2.487(2)
In1–O3#8	2.110(8)	In5–Br2	2.514(2)
In1–O8#7	2.148(8)	As1–O4	1.774(8)
In1–O8#10	2.148(8)	As1–O8#7	1.796(8)
In1–O1	2.213(9)	As1–O7	1.830(8)
In1–O1#5	2.213(9)	As2–O1	1.719(8)
In2–O10	2.133(8)	As2–O7	1.805(9)
In2–O10#4	2.133(8)	As2–O5	1.825(8)
In2–O4#5	2.156(9)	As3–O6	1.758(9)
In2–O4#12	2.156(9)	As3–O3	1.788(8)
In2–O2#10	2.192(8)	As3–O5	1.850(8)
In2–O2#11	2.192(8)	As4–O11#9	1.734(9)
In3–O9	2.110(9)	As4–O10#1	1.782(8)
In3–O2#10	2.135(8)	As4–O12	1.881(9)
In3–O10	2.142(8)	As5–O9#9	1.777(10)
In3–O8#10	2.192(8)	As5–O2	1.780(8)
In3–O1	2.196(8)	As5–O12#9	1.814(8)
In3–O6#6	2.212(8)	O1–In3	2.196(8)
In4–O6#6	2.130(9)	O2–In3#2	2.135(8)
In4–O3	2.151(8)	O4–In2#3	2.156(9)
In4–O4#6	2.152(8)	O5–As3	1.850(8)
In4–O9	2.178(9)	O5–In4	2.341(8)
In4–O12	2.281(9)	O6–In4#6	2.130(9)
In4–O5	2.341(8)	O6–In3#6	2.212(8)
In4–O7#6	2.439(9)	O8–In3#2	2.192(8)
In5–O11	2.025(9)	O10–In3	2.142(8)
In5–Br3	2.483(2)	O12–As4	1.881(9)

[a] Symmetry codes: compound **1**: (#1) $-x + 1, -y + 1, -z + 1$; (#2) $-x, -y, -z + 1$; (#3) $-x, -y + 1, -z + 1$; (#4) $x, y - 1, z$; (#5) $x, y + 1, z$. compound **2**: (#1) $x + 1, y, z$; (#2) $x, y, z + 1$; (#3) $x, y + 1, z$; (#4) $-x, -y, -z$ (#5) $-x, -y + 1, -z$ (#6) $-x + 1, -y + 1, -z$ (#7) $-x, -y + 1, -z + 1$ (#8) $x - 1, y, z$ (#9) $-x + 1, -y, -z + 1$ (#10) $x, y, z - 1$ (#11) $-x, -y, -z + 1$ (#12) $x, y - 1, z$.

tween the zigzag In octahedral chains and consolidate the interlinkage of chains through the formation of $(As_3O_7)^{5-}$ anions (Figure 5, a). The $(As_2O_5)^{4-}$ anions, built of three coordinated As4 and As5 atoms, clamp the In2 atoms and also play a role in consolidating the interlinkage of zigzag chains (Figure 5, b). The O11 atoms coordinated to As4 protrude outside the indium oxide layer, whereas other oxygen atoms are located inside the indium oxide layers. Atom O11 is also coordinated to atom In5, which is also tetrahedrally coordinated by other three bromine atoms with an average In–Br bond length of 2.495(2) Å. The layers are stacked parallel along the *c* direction to yield the crystal structure of **2** (Figure 6).

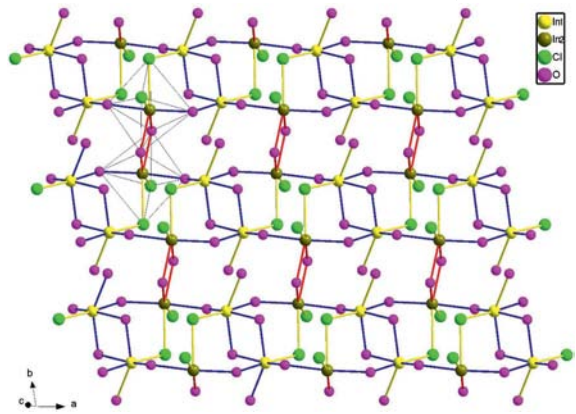

Figure 1. An indium–oxoarsenic–chloride layer parallel to the *ab* plane in **1**. Arsenic atoms are omitted for clarity.

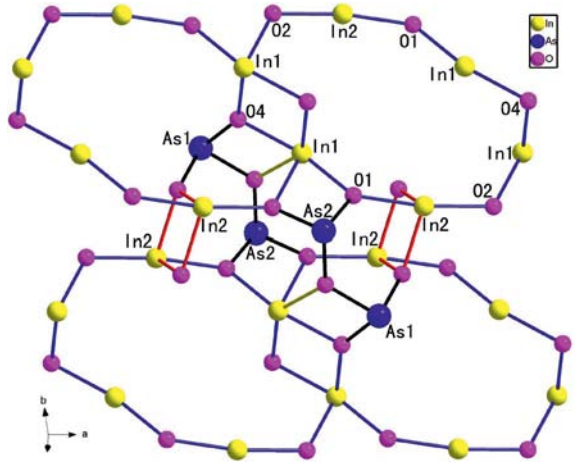

Figure 2. Four 12-membered indium oxide rings are clamped together by $(As_2O_5)^{4-}$ anions. Chlorine atoms are omitted for clarity.

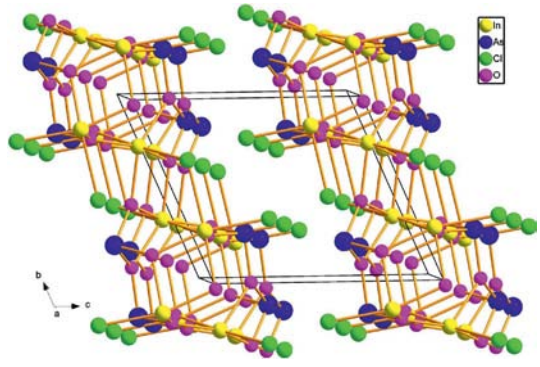

Figure 3. View of the crystal structure of **1** along the *a* direction.

There are three different indium-ion coordination geometries in **2**: octahedrally coordinated In1, In2, and In3 ions, seven-coordinate In4 ions, and tetrahedrally coordinated In5 ions. Compound **2** is the first compound to contain three different indium-ion coordination geometries.

The two compounds both contain an arsenic-oxide group $(As_2O_5)^{4-}$, which is composed of two corner-sharing $[AsO_3E]$ (E = lone pair). In **1**, four of the five oxygen atoms

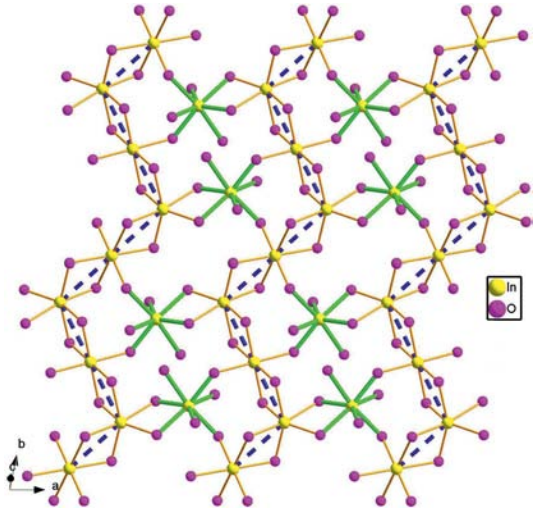

Figure 4. A 2D indium oxide layer parallel to the *ab* plane in **2**. Arsenic atoms and [In5Br$_3$O] units are omitted for clarity.

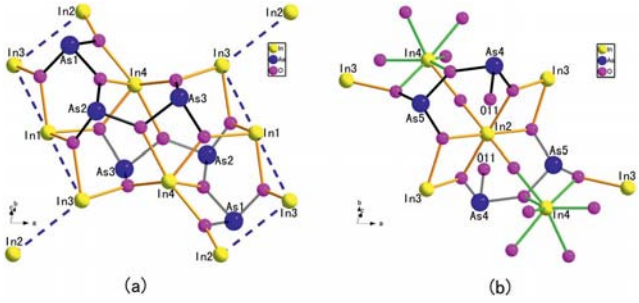

Figure 5. Two zigzag chains are consolidated by (a) two $(As_3O_7)^{5-}$ anions and also by (b) two $(As_2O_5)^{4-}$ anions that clamp In2.

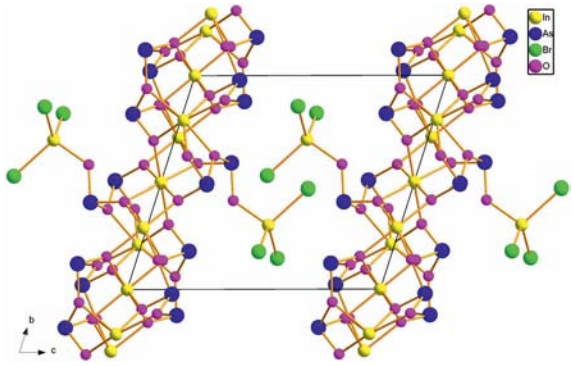

Figure 6. View of the crystal structure of **2** along the *a* direction.

of each $(As_2O_5)^{4-}$ anion (O1, O2, O4, and O5) are bonded to two indium atoms, the remaining one (O3) to only one (Figure 7, a). The $(As_2O_5)^{4-}$ anion in **2** has a similar configuration to that in **1** but has a different coordination environment. Three oxygen atoms (O2, O9, and O10) are bonded to two indium atoms, and two oxygen atoms (O11 and O12) are bonded to only one indium atom (Figure 7, b). Another type of arsenic-oxide group, $(As_3O_7)^{5-}$, also exists in **2**. Three polyhedral [AsO$_3$E] corner-share with each other to form a V-type $(As_3O_7)^{5-}$ polyanion, which is rare in the metal–oxoarsenate(III) system. The only known examples are $Eu_3Zn(As_3O_7)(AsO_3)_2$ and $Eu_6Fe_5(As_4O_9)_2(As_3O_7)_2(AsO_3)_2$.[12] The $(As_2O_5)^{4-}$ ion can be found in a metal–oxoarsenate(III) system,[13] but only $Pb_8(As_2O_5)_2OCl_6$[9e] in metal–oxoarsenate(III)–halide system has been reported. Five of the seven oxygen atoms of each $(As_3O_7)^{5-}$ ion (O1, O3, O4, O6, and O8) are bonded to two indium atoms, and the remaining two (O5 and O7) to only one (Figure 7, c). The As–O bond lengths in the $(As_2O_5)^{4-}$ and $(As_3O_7)^{5-}$ ions in the two compounds range from 1.719(8) to 1.912(7) Å, which are close to those found in the literature.[9,10]

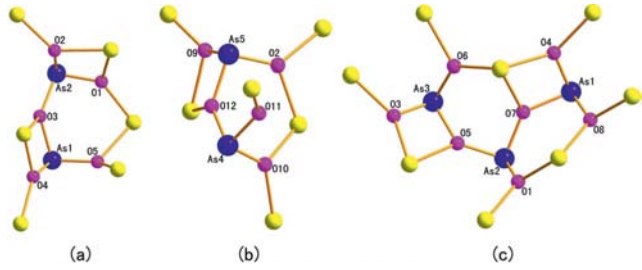

Figure 7. Coordination of (a) $(As_2O_5)^{4-}$ in **1**, (b) $(As_2O_5)^{4-}$ in **2**, and (c) $(As_3O_7)^{5-}$ in **2**. Yellow sphere: indium.

The lone pairs E and the halogen ions are located toward the space available between the In–O layers in **1** and **2**, and these compounds provide new examples in which lone-pair–lone-pair and lone-pair–halogen interactions are observed. The effect of the clusterization of lone electron pairs of As^{3+} cations in **1** and **2** plays a very important role in bringing the layers together. Each layer can thus be considered an infinite two-dimensional molecule. On the other hand, layer-structure compounds **1** and **2** can be regarded as quantum well materials and may be potentially applied in diode lasers and photodetectors.

Thermogravimetric Analyses (TGA)

TGA curves indicate that compounds **1** and **2** are stable up to about 500 and 530 °C, respectively (Figure 8). They both exhibit two main steps of weight losses. For **1**, the first one occurred in the temperature range of 500–640 °C, which corresponds to the release of 0.78 molecule of As_2O_3 and 0.43 molecule of $AsCl_3$. The observed weight loss and calculated value are both 44.0%. Above 650 °C, it is further decomposed, which corresponds to the release of 0.24 molecule of $InCl_3$. The total weight loss at 1000 °C is 55.0%, which agrees with the calculated value of the final residue In_2O_3 (46.1%). The final residue In_2O_3 can be identified by powder XRD (Figure S4 in the Supporting Information) and energy-dispersive X-ray spectroscopy (EDS). The EDS measurements of the final residues of **1** and **2** show that both of them contain only elements oxygen and indium in a ratio of about 3:2. The first decomposition step of **2** occurred in the temperature range of 530–650 °C, which corresponds to the release of one As_2O_3 and $AsBr_3$. The observed weight loss (40.8%) is close to the calculated value

42.0%. Above 650 °C, it is further decomposed, which corresponds to the release of another As_2O_3. The total weight loss at 1000 °C is 55.0%, which agrees with the calculated value of the final residue In_2O_3 (44.2%). No obvious melting peaks were found before thermal decomposition of the two compounds on the differential thermal analysis (DTA) spectra.

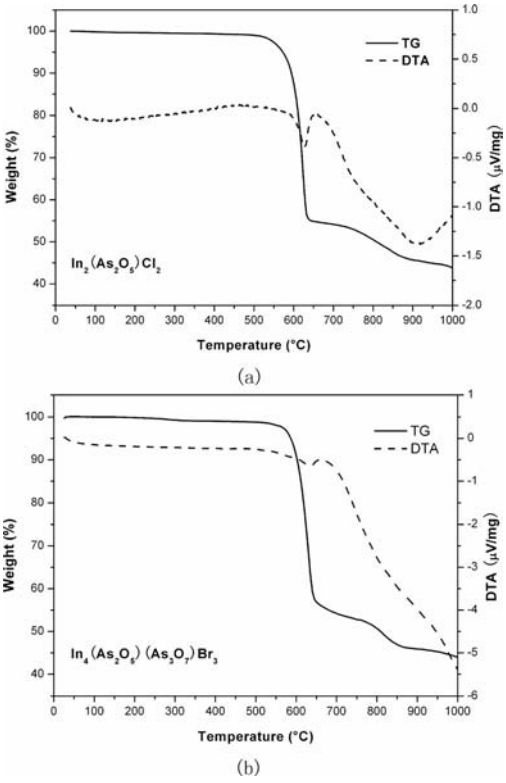

Figure 8. TG/DTA curves for (a) **1** and (b) **2**.

IR and Optical Spectrum Studies

IR studies indicate that compounds **1** and **2** are transparent in the range of 4000–1000 cm^{-1} (see Figure S6 in the Supporting Information). Compared with the IR spectra of As_2O_3 and In_2O_3, the absorption bands of **1** at 479, 764, and 779 cm^{-1} can be assigned to the ν(As–O) vibrations, and those at 423, 582, 625, and 642 cm^{-1} can be attributed to the ν(As–O–In) vibrations. The absorption bands of **2** at 481, 740, 767, and 804 cm^{-1} are characteristic of the ν(As–O) vibrations, whereas those at 463, 548, and 604 originate from the ν(As–O–In) vibrations, and bands at 627 and 665 cm^{-1} are due to the ν(As–O–In) vibrations. Optical diffuse reflectance spectra of **1** and **2** reveal optical band gaps of 4.62 and 4.22 eV, respectively (Figure 9). Hence, both compounds are wide-band-gap semiconductors. The photoluminescent (PL) spectra of **1** and **2** were studied in the solid state at room temperature, and their emission and excitation spectra are depicted in Figure S5. Compound **1** displays three photoluminescent emission bands at 426, 460, and 556 nm upon excitation at 324 nm, and compound **2** displays only a very weak broad emission band at 535 nm upon excitation at 336 nm.

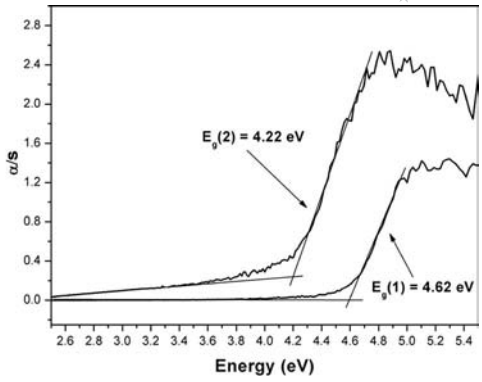

Figure 9. Room-temperature optical absorption spectra for **1** and **2**.

Theoretical Studies

The calculated band structures as well as density of states (DOS) of **1** and **2** along certain symmetry directions (Table 4) are given in Figure 10. It can be noted from the band-structure plots that compounds **1** and **2** are both indirect band-gap materials. The calculated band gaps of **1** and **2** using the local density approximation (LDA) are E_g = 3.40 and 3.08 eV, which are smaller than the experimental values 4.62 and 4.22 eV, respectively. So the scissors operator of 1.22 and 1.14 eV have been obtained for calculations of DOS as well as dielectric functions of **1** and **2**, respectively.

Table 4. The state energies [eV] of the lowest conduction band (L-CB) and the highest valence band (H-VB) at some *k* points in the Brillouin zone of **1** and **2**.

k point	L-CB	H-VB
1		
G(0.0, 0.0, 0.0)	3.46329	–0.00651
F(0.0, 0.5, 0.0)	3.88924	–0.08894
Q(0.0, 0.5, 0.5)	3.79199	–0.01516
Z(0.0, 0.0, 0.5)	3.39642	–0.13567
2		
G(0.0, 0.0, 0.0)	3.08207	–0.05875
F(0.0, 0.5, 0.0)	3.30503	–0.03265
Q(0.0, 0.5, 0.5)	3.29031	–0.01953
Z(0.0, 0.0, 0.5)	3.16035	0.0

From DOS and partial density of states (PDOS) diagrams, it is known that for **1**, the conductive band (CB) is mainly derived from As 4p states mixed with small amounts of In 5s, In 5p, O 2s, and O 2p states, whereas the valence band (VB) from –11.0 eV to the Fermi level is composed of Cl 3p and O 2p states mixed with small amounts of As 4s, As 4p, In 5s, and In 5p states. The band from –20.0 to –11.0 eV originates predominately from Cl 3s and O 2s states, as well as small portion of As 4s and As 4p states. Therefore, their optical absorptions can mainly be ascribed to the charge transitions from Cl 3p and O 2p states to As 4p states. For **2**, The As 4p states, mixed with small In 5s, In 5p, O 2s, and O 2p states, create the CBs between the Fermi level (0.0 eV) and energy 6.0 eV. The VBs between

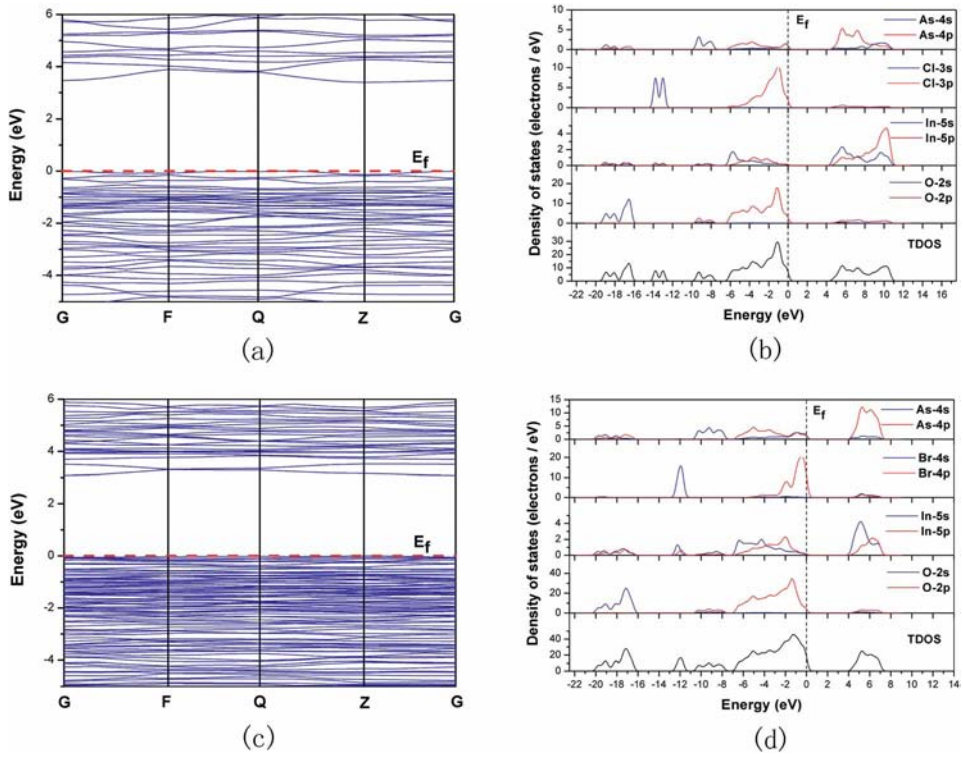

Figure 10. (a) Band structures of **1** and (c) **2**. Bands are shown only between –5.0 and 6.0 eV for clarity. (b) Total and partial density of states of **1** and (d) **2**. The energies less than –22.5 eV are omitted for clarity. The Fermi level is set at 0 eV for all the band structures and DOS.

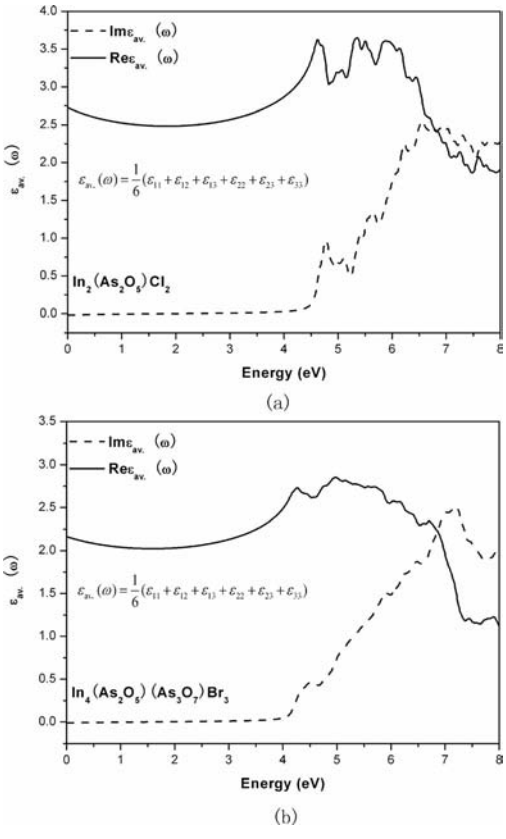

Figure 11. Calculated imaginary and real parts of average dielectric functions of (a) **1** and (b) **2**.

–11.0 eV and Fermi level are mostly formed by Br 4p and O 2p states mixed with a small amount of As 4s, As 4p, In 5s, and In 5p states; and the VBs between energy –20.0 and –11.0 eV are mostly a contribution from Br 4s and O 2s states hybridized with a small amount of As 4s, As 4p, In 5s, and In 5p states. Therefore, the optical absorptions of **2** are mainly ascribed to the charge transitions from Br 4p and O 2p states to As 4p states.

The calculated imaginary part $Im\varepsilon_{av.}(\omega)$ and real part $Re\varepsilon_{av.}(\omega)$ of the average frequency-dependent dielectric functions of **1** and **2** are in Figure 11. It is found from the dispersion of the calculated $Im\varepsilon_{av.}(\omega)$ spectra that the maximum absorption peaks are located at about 4.78, 5.10, 5.63, 6.22, and 6.56 eV for **1**, and 4.50, 5.90, and 7.20 eV for **2** in *x*, *y*, and *z* polarization directions, which are contributions from the charge transfers from Cl 3p and O 2p states to As 4p states, and from Br 4p and O 2p states to O 2p states, respectively, according to the above DOS analysis.

Conclusion

In conclusion, the syntheses, crystal and band structures, and optical properties of the first two oxoarsenate(III) chlorides of indium, $In_2(As_2O_5)Cl_2$ (**1**) and $In_4(As_2O_5)(As_3O_7)Br_3$ (**2**), have been described. Both of the compounds feature layered structures, in which indium–oxide halide octahedral rings or indium–oxo chains are bridged by indium–oxide halide octahedral dimers or indium–oxo unicapped trigonal prisms, and the interlinkage between the rings or

chains are also consolidated by $(As_2O_5)^{4-}$ anions, or $(As_2O_5)^{4-}$ and $(As_3O_7)^{5-}$ anions. The In^{3+} cations in **2** adopt there different types of coordination geometries, coordinated by O^{2-}, and Br^- to form $[InO_6]$, $[InO_7]$, and $[InOBr_3]$ units, which is very rare in the reported indium compounds. Both compounds are wide indirect band-gap semiconductors based on experimental measurements and electronic band-structure calculations. It is observed that the sharp absorption peaks for **1** and **2** mainly originate from the charge transfer from Cl 3p or Br 4p and O 2p states to As 4p states.

Experimental Section

Reagents and Syntheses: As_2O_3 was prepared directly by the combustion reaction of As_2S_3 (99.999%) in oxygen. SO_2 gas was absorbed by saturated sodium hydroxide solution, and the purified As_2O_3 was obtained by distilling the product for several times. $InBr_3$ is prepared directly by the reaction of indium powder (99.99%) and liquid bromine (99.5%) dried by concentrated sulfuric acid. Liquid bromine must be added in excess amounts, and the reactor with magnetic stirring is heated to about 80 °C in a water bath to make sure that all indium powder is transformed into $InBr_3$. The purities of As_2O_3 and $InBr_3$ were confirmed by an X-ray diffraction (XRD) study (see Figure S1 in the Supporting Information). Some peaks found on the powder XRD pattern of prepared $InBr_3$ are not attributed to any reported binary compounds that contain indium and bromine, which may be because of the existence of unknown compounds that contain indium and bromine. Furthermore, the purity of $InBr_3$ was precisely determined to be 99.05% with an inductively coupled plasma (ICP) OES spectrometer.

Caution! As_2S_3 and As_2O_3 are very toxic, and the preparation of $InBr_3$ involves the use of liquid bromine and concentrated sulfuric acid, both of which are very corrosive. Experiments must be performed in a ventilated cabinet and extreme care must be exercised. $InBr_3$ is water-sensitive and its preparation and preservation must be in dry environment.

Single crystals of **1** and **2** were obtained by solid-state reactions with a yield of more than 90% for both compounds. Compound **1** was crystallized from the reaction of In_2O_3 (1.0 mmol, 99.5%), As_2O_3 (1.5 mmol, 99.5%), and $InCl_3$ (1.0 mmol, 99.99%). Compound **2** was crystallized from the reaction of In_2O_3 (1.5 mmol, 99.5%), As_2O_3 (2.5 mmol, 99.5%), and $InBr_3$ (1.0 mmol, 99.05%). The starting materials were ground into fine powders in an agate mortar and pressed into a pellet in a glovebox, followed by being loaded into Pyrex tubes, evacuated to 1×10^{-4} Torr, and flame-sealed. The tubes were placed into a computer-controlled furnace, heated from room temperature to 300 °C at a rate of 50 °C per hour and kept at 300 °C for 2 d. They were heated to 700 °C at 20 °C per hour and kept at 700 °C for 2 d, slowly cooled to 100 °C at a rate of 2.5 °C per hour and then finally cooled to room temperature in 5 h. Colorless flakelike crystals of **1** and **2** were handpicked under a microscope, and their purities were confirmed by an X-ray diffraction (XRD) study (Figure S2 in the Supporting Information). They are stable in the presence of air and water.

Crystal Structure Determination: For **1** and **2**, single crystals with dimensions of $0.1 \times 0.05 \times 0.01$ and $0.15 \times 0.10 \times 0.02$ mm^3, respectively, were mounted on glass fiber for single-crystal X-ray diffraction analysis. The measurements were performed with a Rigaku Mercury CCD diffractometer equipped with graphite-monochromated Mo-K_α radiation (λ = 0.71073 Å) at 293 K. The intensity data sets were collected with an ω-scan technique and reduced with CrystalClear software.[14]

The structures of **1** and **2** were solved by direct methods and refined by full-matrix least-squares techniques on F^2 with anisotropic thermal parameters for all atoms. All of the calculations were performed with the Siemens SHELXL version 5 package of crystallographic software.[15] The formulas are based on taking collectively into account crystallographically refined compositions and requirements of charge neutrality.

Further details on the crystal structure investigations may be obtained from the Inorganic Crystal Structure Database (ICSD), Fachinformationszentrum Karlsruhe, 76344 Eggenstein-Leopoldshafen, Germany (fax: +49-7247-808-666; e-mail: crysdata@fiz-karlsruhe.de), on quoting the depository numbers CSD-422701 (for **1**) , -422702 (for **2**).

Powder XRD: The powder XRD patterns were collected with a Rigaku DMAX 2500 diffractometer powered at 40 KV and 100 mA with Cu-K_α radiation (λ = 1.5406 Å) at a scan speed of 5° per minute at room temperature. The simulated patterns were produced with the Mercury program and single-crystal reflection data.

Differential Thermal Analysis (DTA): TG/DTA studies of **1** and **2** were carried out with a NETZSCH STA 449C instrument under a nitrogen atmosphere. The samples and reference were held in Al_2O_3 crucibles, heated at a rate of 10 °C per minute from room temperature to 1000 °C. Thermal decomposition residues of **1** and **2** were examined by powder XRD, performed with a Rigaku DMAX 2500 diffractometer powered at 40 KV and 100 mA with Cu-K_α radiation (λ = 1.5406 Å) at a scan speed of 2° per minute at room temperature, and energy-dispersive X-ray spectroscopy (EDS) performed with a JSM6700F scanning electron microscope (SEM).

Infrared and UV/Vis/NIR Diffuse Reflectance and Photoluminescent Spectroscopies: The diffuse reflectance spectra were recorded at room temperature with a computer-controlled Lambda 900 UV/Vis/NIR spectrometer equipped with an integrating sphere in the wavelength range of 200–2000 nm. A $BaSO_4$ plate was used as a reference, on which the finely ground powders of the samples were coated. The absorption spectra were calculated from reflection spectra by using the Kubelka–Munk function. The IR spectra were recorded with a Nicolet Magana 750 FTIR spectrophotometer in the range of 4000–400 cm^{-1}. Powdery samples were pressed into pellets with KBr. The solid-state photoluminescent excitation and emission spectra were performed with an Edinburgh EI920 fluorescence spectrophotometer equipped with a 450 W steady-state xenon lamp (ozone-free) at room temperature with a wavelength increment of 1.0 nm and integration time of 1.0 s. When performing PL measurements, a 200–400 nm band-pass and 395 nm high-pass filter were applied.

Computational Procedures: The crystallographic data of **1** and **2** determined by single-crystal X-ray diffraction analysis were used to calculate their electronic band structure and optical properties. The calculation of the electronic band structures, densities of state (DOS), and dielectric functions were performed with the ABINIT computer code package.[16] Theoretical calculations were carried out using the Fritz-Haber-Institute (FHI) pseudopotentials scheme (Troullier–Martins Scheme[17]) with a plane-wave energy cutoff of 20 Hartree for **1** and **2**. A $4 \times 4 \times 3$ Monkhorst–Pack grid of Brillouin-zone k-point sampling was used in the calculations for **1** and $3 \times 3 \times 2$ for **2**. The exchange and correlation effects were treated by the local-density approximation in the Ceperley–Alder form

with the Perdew–Wang parameterization.[18] The convergences of the calculated properties were verified with respect to the *k*-point sampling and plane-wave energy cutoff.

In the calculation of dielectric functions and the density of states (DOS) of **1** and **2**, scissors operators of 1.22 and 1.14 eV were applied for **1** and **2**, respectively, and more than 130 empty bands were used for **1** and 60 for **2**.

Supporting Information (see footnote on the first page of this article): XRD powder patterns of prepared As_2O_3, $InBr_3$, **1**, and **2**, and the residues of DTA of **1** and **2**, coordination geometries, solid-state emission spectra, FTIR spectra, and UV diffuse reflectance spectra of **1** and **2**.

Acknowledgments

We gratefully acknowledge financial support from the National Natural Science Foundation of China (NSFC) (90922035, 21003126), 973 program (2011CBA00505), the Key Project from the CAS (KJCX2.YW.M10), and the National Science Foundation (NSF) of Fujian Province (2008I0026, 2008F3115).

[1] a) L. Mihaly, T. Feher, B. Dora, B. Nafradi, H. Berger, L. Forro, *Phys. Rev. B* **2006**, *74*, 174403; b) P. Lemmens, K. Y. Choi, G. Guntherodt, M. Millet, P. Johnsson, F. Mila, R. Valenti, C. Gros, W. Brenig, *Phys. B: Condens. Matter* **2003**, *329–333*, 1049–1050; c) E. Ma, H. L. Jiang, *Chin. J. Struct. Chem.* **2007**, *26*, 1159–1164.

[2] a) Y. Porter, N. S. P. Bhuvanesh, P. S. Halasyamani, *Inorg. Chem.* **2001**, *40*, 1172–1175; b) F. Kong, S.-P. Huang, Z.-M. Sun, J.-G. Mao, W.-D. Cheng, *J. Am. Chem. Soc.* **2006**, *128*, 7750–7751; c) Y. Porter, K. M. Ok, N. S. P. Bhuvanesh, P. S. Halasyamani, *Chem. Mater.* **2001**, *13*, 1910–1915; d) K. M. Ok, N. S. P. Bhuvanesh, P. S. Halasyamani, *Inorg. Chem.* **2001**, *40*, 1978–1980.

[3] J.-G. Mao, H.-L. Jiang, F. Kong, *Inorg. Chem.* **2008**, *47*, 8498–8510, and references cited therein.

[4] R. Takagi, M. Johnsson, R. K. Kremer, P. Lemmens, *J. Solid State Chem.* **2006**, *179*, 3763–3767.

[5] a) R. Valenti, T. Saha-Dasgupta, H. O. Jeschke, B. Rahaman, H. Rosner, P. Lemmens, R. Takagi, M. Johnsson, *Phys. C* **2007**, *460–462*, 462–463; b) M. Johnsson, K. W. Tornroos, P. Lemmens, P. Millet, *Chem. Mater.* **2003**, *15*, 68–73; c) R. Becker, H. Berger, M. Johnsson, M. Prester, Z. Marohnic, M. Miljak, M. Herak, *J. Solid State Chem.* **2006**, *179*, 836–842; d) R. Becker, M. Prester, H. Berger, M. Johnsson, D. Drobac, I. Zivkovic, *Solid State Sci.* **2007**, *9*, 223–230; e) R. Becker, M. Prester, H. Berger, P. H. Lin, M. Johnsson, D. Drobac, I. Zivkovic, *J. Solid State Chem.* **2007**, *180*, 1051–1059; f) R. Becker, M. Johnsson, R. K. Kremer, H. H. Klauss, P. Lemmens, *J. Am. Chem. Soc.* **2006**, *128*, 15469–15475.

[6] a) E. O. Chi, K. M. Ok, Y. Porter, P. S. Halasyamani, *Chem. Mater.* **2006**, *18*, 2070–2074; b) J. Goodey, J. Broussard, P. S. Halasyamani, *Chem. Mater.* **2002**, *14*, 3174–3180; c) U. Kortz, M. G. Savelieff, F. Y. A. Ghali, L. M. Khalil, S. M. Maalouf, D. I. Sinno, *Angew. Chem. Int. Ed.* **2002**, *41*, 4070–4073; d) H. S. Ra, K. M. Ok, P. S. Halasyamani, *J. Am. Chem. Soc.* **2003**, *125*, 7764–7765.

[7] H. L. Jiang, E. Ma, J. G. Mao, *Inorg. Chem.* **2007**, *46*, 7012–7023.

[8] a) P. S. Halasyamani, K. R. Poeppelmeier, *Chem. Mater.* **1998**, *10*, 2753–2769.

[9] a) F. Pertlik, *Monatsh. Chem.* **1988**, *119*, 451–456; b) F. Z. Pertlik, *Kristallogr.* **1988**, *184*, 191–201; c) H. Effenberger, F. Pertlik, *Tschermaks Mineral. Petrogr. Mitt.* **1979**, *26*, 95–107; d) T. Baikie, C. Ferraris, W. T. Klooster, S. Madhavi, S. S. Pramana, A. Pring, G. Schmidt, T. White, *J. Acta Crystallogr., Sect. B: Struct. Sci.* **2008**, *64*, 34–41; e) F. Pertlik, *Monatsh. Chem.* **1986**, *117*, 1257–1261; f) M. Ben Hamida, M. S. Wickleder, *Z. Anorg. Allg. Chem.* **2006**, *632*, 2195–2197.

[10] a) D.-H. Kang, Th. Komm, Th. Schleid, *Z. Kristallogr.* **2005**, *Suppl.*, *22*, 157; b) H. Ben Yahia, A. Villesuzanne, U. C. Rodewald, T. Schleid, R. Z. Pottgen, *Z. Naturforsch. Sect. B* **2010**, *65*, 549–555; c) D. H. Kang, J. Wontcheu, T. Schleid, *Solid State Sci.* **2009**, *11*, 299–304; d) H. Ben Yahia, U. C. Rodewald, R. Pottgen, *Naturforsch. Sect. B* **2009**, *64*, 896–900; e) R. Klaska, W. Gebert, *Z. Kristallogr.* **1982**, *159*, 75–76; f) F. Pertlik, *Miner. Petrol.* **1987**, *36*, 85–92.

[11] a) C. T. Prewitt, R. D. Shannon, D. B. Rogers, W. W. Sleight, *Inorg. Chem.* **1969**, *8*, 1985–1993; b) N. Nadaud, N. Lequeux, M. Nanot, J. Jove, T. Roisnel, *J. Solid State Chem.* **1998**, *135*, 140–148.

[12] M. Ben Hamida, M. S. Wickleder, *Z. Anorg. Allg. Chem.* **2006**, *632*, 2109.

[13] a) M. Ben Hamida, C. Warns, M. S. Wickleder, *Z. Naturforsch., Teil B* **2005**, *60*, 1219–1223; b) D.-H. Kang, Th. Schleid, *Z. Anorg. Allg. Chem.* **2006**, *632*, 91–96.

[14] *CrystalClear*, v. 1.3.5, Rigaku Corporation, Tokyo, **2002**.

[15] *SHELXLTL*, v. 5, reference manual, Siemens Energy & Automation Inc., Madison, WI, **1994**.

[16] a) X. Gonze, J.-M. Beuken, R. Caracas, F. Detraux, M. Fuchs, G.-M. Rignanese, L. Sindic, M. Verstraete, G. Zerah, F. Jollet, M. Torrent, A. Roy, M. Mikami, P. Ghosez, J.-Y. Raty, D. C. Allan, *Comput. Mater. Sci.* **2002**, *25*, 478–492; b) X. Gonze, G.-M. Rignanese, M. Verstraete, J.-M. Beuken, Y. Pouillon, R. Caracas, F. Jollet, M. Torrent, G. Zerah, M. Mikami, P. Ghosez, M. Veithen, J.-Y. Raty, V. Olevano, F. Bruneval, L. Reining, R. Godby, G. Onida, D. R. Hamann, D. C. Allan, *Z. Kristallogr.* **2005**, *220*, 558–562; c) the ABINIT code is a common project of the Université Catholique de Louvain, Corning Incorporated, and other contributors (URL: http://www.abinit.org); d) S. Goedecker, *SIAM J. Sci. Comput.* **1997**, *18*, 1605–1611; e) M. C. Payne, M. P. Teter, D. C. Allan, T. A. Arias, J. D. Joannopoulos, *Rev. Mod. Phys.* **1992**, *64*, 1045–1097; f) X. Gonze, *Phys. Rev. B* **1996**, *54*, 4383–4386; g) M. Fuchs, M. Scheffler, *Comput. Phys. Commun*. **1999**, *119*, 67–98; h) C. Lee, X. Gonze, *Phys. Rev. B* **1995**, *51*, 8610–8613.

[17] D. Vanderbilt, *Phys. Rev. B* **1990**, *41*, 7892–7895.

[18] a) D. Ceperley, D. M. Ceperley, *Phys. Rev. B* **1978**, *18*, 3126–3138; b) D. M. Ceperley, B. Alder, *J. Phys. Rev. Lett.* **1980**, *45*, 566–569; c) J. P. Perdew, Y. Wang, *Phys. Rev. B* **1992**, *45*, 13244–13249.

Received: January 26, 2011
Published Online: May 6, 2011

